

Mass Conservative Reduced Order Modeling of a Free Boundary Osmotic Cell Swelling Problem

Christoph Lehrenfeld^a and Stephan Rave^b

^aInstitute for Numerical and Applied Mathematics, University of
Göttingen, lehrenfeld@math.uni-goettingen.de

^bApplied Mathematics, University of Münster,
stephan.rave@uni-muenster.de

May 4, 2018

Abstract

We consider model order reduction for a free boundary problem of an osmotic cell that is parameterized by material parameters as well as the initial shape of the cell. Our approach is based on an Arbitrary-Lagrangian-Eulerian description of the model that is discretized by a mass-conservative finite element scheme. Using reduced basis techniques and empirical interpolation, we construct a parameterized reduced order model in which the mass conservation property of the full-order model is exactly preserved. Numerical experiments are provided that highlight the performance of the resulting reduced order model.

1 Introduction

Free boundary problems are PDE problems that involve an a priori unknown (free) interface or boundary. These type of problems arise in different applications from physics, engineering, finance and biology. Let us mention a few important application fields where free boundary problems play an important role. In physics and engineering, many situations where different fluids (or solids) are involved, e.g. water and oil in petroleum problems, can be cast into free boundary problems as in the classical Stefan problem [32]; In finance, optimal stopping of stochastic processes is often solved by reduction to free boundary problems [24], and in biology, the mathematical modeling of problems like tumor growth and wound healing leads to free boundary problems [9].

While projection-based reduced order modeling techniques such as reduced basis methods have been successfully applied to a wide variety of PDE models (see, e.g., [26, 12, 6] for an overview), the reduction of problems that involve an evolving geometry $\Omega(t)$ remains challenging: Whereas traditional reduction methods are built around the idea of finding a joint linear approximation space for the entire manifold

of solution state vectors, the solutions $u(t)$ of free boundary problems naturally lie in time-dependent function spaces $V(t)$ that depend on the a priori unknown evolution of $\Omega(t)$.

Taking an Eulerian point of view, a naive approach to resolve this issue is to consider linear embeddings $\Lambda(t)$ of $V(t)$ into a larger space V of (discontinuous) functions on some $\Omega^* \supset \bigcup_t \Omega(t)$ by extending the functions with zero on the complement of $\Omega(t)$, and then search for a reduced approximation space $V_N \subset V$ for the solution manifold $\mathcal{M}_V := \{\Lambda(t)(u(t))\}$. However, as is well-known from hyperbolic problems with traveling shocks, the moving jump at the boundary of $\Omega(t)$ leads to a slow decay of the Kolmogorov n -widths of \mathcal{M}_V (e.g. [22]). Thus, a good low-dimensional linear approximation space V_N for \mathcal{M}_V cannot exist.

Following ideas from [21], the aim of this paper is to approach this problem by considering nonlinear approximations of \mathcal{M}_V where we allow transformations of functions f in V_N of the form $\Psi.f(x) := f(\Psi(x))$ with some diffeomorphism Ψ of Ω^* . If the functions $\Psi(t)$ are chosen such that the supports of functions in $\hat{\mathcal{M}}_V := \{\Psi(t).\Lambda(t)(u(t))\}$ have a fixed boundary, the n -widths of $\hat{\mathcal{M}}_V$ will decay fast. Given a good approximation space V_N of $\hat{\mathcal{M}}_V$, $\Psi(t)^{-1}.V_N$ will then yield good approximations of $\Lambda(t)(u(t))$. Noting that such transformations $\Psi(t)$ induce mappings of a fixed reference domain $\hat{\Omega}$ to $\Omega(t)$, this leads us to reformulate the original problem on $\hat{\Omega}$ and introduce $\Psi(t)$ (as a function of $\hat{\Omega}$) as an additional solution field. The evolution of $\Psi(t)$ will be determined by the evolution of the boundary $\Gamma(t)$ of $\Omega(t)$ as given by the free boundary problem and an harmonic extension into $\hat{\Omega}$. In effect, we arrive at a formulation of the free boundary problem on the reference-domain using the domain transformation $\Psi(t)$ as in Arbitrary-Lagrangian-Eulerian (ALE) methods [14, 8]. The freedom in choice of the harmonic extension to determine $\Psi(t)$ can be seen in analogy to choosing a phase condition in context of the freezing formulation discussed in [21].

Literature on model order reduction for free boundary problems seems to be mostly non-existent. We are only aware of the preliminary work in [13] and the following related works. In the context of fluid-structure interaction (FSI) problems a similar ALE formulation has been considered in [3]. The use of a reference domain for the reduction of models with parametrized geometry dates back to the early days of reduced basis methods, e.g. [25]. This approach has been extended to FSI problems in [15]. An increasingly popular way to deal with moving domains is based on an implicit description of the geometry through indicator functions (e.g. level sets [30, 23]) as it often allows for a higher flexibility of the geometry handling w.r.t. large deformations and topology changes. A nonlinear approximation method based on the truncation of functions in V_N via time-dependent indicator functions is discussed in [2]. Due to the lack of hyperreduction no fully online-efficient reduced order model (ROM) is obtained, however. Model order reduction of phase-field models, in which $\Gamma(t)$ is approximated by an easier-to-approximate diffuse interface layer, is discussed in [34, 28, 11].

Despite the high accuracy of projection-based ROMs, conservation properties of the original PDE model are usually only approximately preserved by the reduction process. The exact conservation of quantities such as the total mass of the system is often of particular interest, however. In this work we will derive globally mass conserving ROMs based on a carefully chosen finite element discretization of the free

boundary problem in which the mass conservation constraint is implemented by testing the variational formulation with a constant function. Including the constant functions in the reduced space then ensures mass conservation of the Galerkin ROM. To preserve this property under empirical interpolation [5], we propose a rank-one modification of the interpolated mass matrix to ensure exact yet efficient assembly of the constraint.

The inclusion of locally constant test functions in the reduced space to obtain locally mass conservative flux reconstructions is considered in [20] to improve the efficiency of a localized a posteriori error estimator in the context of localized model order reduction. In [7] an alternative approach to preserve conservation properties is presented, which is based on the inclusion of additional constraints in the least-squares Petrov-Galerkin minimization problem that is solved in the ROM.

Content and structure of the paper

The paper is structured as follows. We introduce a mathematical model for osmotic cell swelling as a model problem in Section 2. The Arbitrary-Lagrangian-Eulerian formulation of the full order model is then discussed in Section 3 before we apply model order reduction in Section 4. Based on the numerical experiments in Section 5, we discuss the performance and potential of this approach before we conclude.

2 Mathematical model of an osmotic cell swelling problem

As a model free boundary problem we consider a mathematical model of osmotic cell swelling that is also considered in a.o. [17, 27, 10, 36, 37, 38]. A membrane separates the interior of a cell which is filled with a fluid from the outside. Inside and outside of the cell a solute concentration is dissolved to which the membrane is impermeable. The outer concentration is assumed to be constant and known. An extension to the “two-phase” osmosis problem where the outer concentration field is also considered to be unknown can be found in [18, 27]. We, however, restrict to the simpler “one-phase” case. In this system, the membrane is subject to two acting forces: on the one hand, a surface tension force that only depends on the shape of the membrane and counteracts large curvatures; on the other hand, a force induced by the tendency to equilibrate the solute concentration across the membrane. The latter is modeled by Van’t Hoff’s law, which states that the pressure at the boundary is proportional to the concentration difference at the free boundary.

Let us denote by u the solute concentration. Inside the cell, u is subject to a linear unsteady diffusion equation with constant diffusion coefficient α . Boundary conditions result naturally from the conservation of mass principle as the total solute concentration is constant. Let $(0, T]$, $T > 0$ be the time interval of interest and $\Omega_0 \subset \mathbb{R}^d$, $d = 2, 3$ be the initial domain of the cell with $\Gamma_0 := \partial\Omega_0$ the initial shape of the membrane. Then, the model for the solute concentration and the boundary

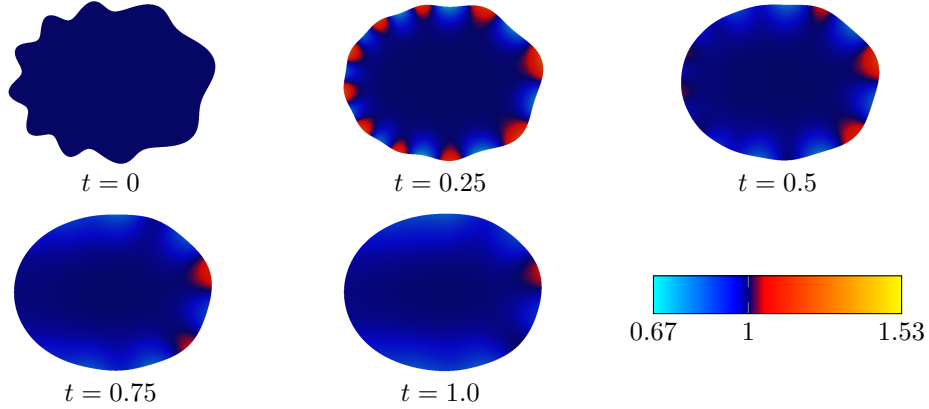


Figure 1: Evolution of cell geometry and concentration for an example considered in Section 5.2: The initially homogeneous distribution of the concentration is given in the initial cell shape. The mean curvature smoothens the cell shape, which leads to local changes in the concentration field. Finally, the evolution tends to a stationary state which is a circle with a homogeneous distribution of the concentration.

motion is given by

$$\partial_t u - \alpha \Delta u = 0 \quad \text{in } \Omega(t), \quad (1a)$$

$$w_\Gamma u + \alpha \partial_{\mathbf{n}} u = 0 \quad \text{on } \Gamma(t), \quad (1b)$$

$$-\beta \kappa + \gamma(u - u_{\text{ext}}) = w_\Gamma \quad \text{on } \Gamma(t). \quad (1c)$$

Here, w_Γ is the velocity (in normal direction) of the boundary $\Gamma(t) := \partial\Omega(t)$. With the mean curvature κ (positive for convex domains) the first term $-\beta\kappa$ in (1c) models the effect of surface tension, whereas $\gamma(u - u_{\text{ext}})$ models the effect of the osmotic pressure. The constants β and γ are material constants depending only on the membrane and the solute. $\partial_{\mathbf{n}} u$ is the normal derivative of u with \mathbf{n} the outer normal to $\Omega(t)$.

With Reynolds' transport theorem we easily see that (1b) implies conservation of the total solute:

$$\frac{d}{dt} \int_{\Omega(t)} u \, d\mathbf{x} = \int_{\Omega(t)} \underbrace{\partial_t u}_{=\alpha \Delta u} \, d\mathbf{x} + \int_{\Gamma(t)} w_\Gamma u \, d\mathbf{s} = \int_{\Gamma(t)} \alpha \partial_{\mathbf{n}} u + w_\Gamma u \, d\mathbf{s} = 0. \quad (2)$$

We notice that in the model a higher concentration at the boundary of the cell introduces a force that tends to expand the cell. The surface tension force typically has the opposite tendency. For convex domains it tends to compress the cell. Note that in this model the domain Ω cannot degenerate. This is due to the fact that the boundary condition (1b) ensures conservation of the total solute concentration so that the concentration increases if the cell shrinks. In the case of a shrinking cell, the concentration will eventually reach a level where the second term in (1c) compensates

the surface tension force. For an initially simple connected domain Ω_0 the system tends towards the stationary solution of (1) which has a spherical shaped domain Ω_∞ with a constant concentration u_∞ . In Figure 1 an example evolution is shown.

3 Arbitrary-Lagrangian-Eulerian-based finite element discretization

In this section we derive a discretization method for the osmotic cell swelling problem based on an Arbitrary-Lagrangian-Eulerian (ALE) description [14, 8] and a finite element discretization. To this end, we first introduce the geometry description and a decomposition of the coupled problem into subproblems on the continuous level in Section 3.1. In Section 3.2 we introduce some notation and a decoupling scheme consisting of discrete subproblems, the treatment of which is discussed one after another in Sections 3.3 – 3.5. The conservation property (2) is ensured on the discrete level in the discretization of the time stepping for the concentration field in Section 3.5.

3.1 ALE formulation of the continuous problem

3.1.1 Geometry description through mappings

In an ALE description we deal with the fact that the domain is moving in time by introducing a reference configuration $\hat{\Omega}$ and describe $\Omega(t)$ by a time-dependent transformation

$$\Psi : \hat{\Omega} \times [0, T] \rightarrow \mathbb{R}^d. \quad (3)$$

By $\mathbf{w} = \partial_t \Psi$ we denote the mesh velocity. With abuse of notation, we write $\Psi(t)$ for the restriction of Ψ to a fixed time t , i.e. the purely spatial function $\Psi(t) : \hat{\Omega} \rightarrow \Omega(t)$.

3.1.2 A generic extension from boundary transformation to volume transformation

For the notation of restrictions of functions to the boundary Γ we use a subindex, e.g. $\Psi_\Gamma = \Psi|_\Gamma$. The evolution of the domain is determined by (1c),

$$\partial_t \Psi_\Gamma = w_\Gamma \mathbf{n} = -\beta\kappa \mathbf{n} + \gamma(u - u_{\text{ext}}) \mathbf{n} \quad \text{on } \Gamma(t). \quad (4)$$

To determine the mesh transformation $\Psi(t)$ in the volume we use a linear extension operator $\mathcal{E} : (H^{\frac{1}{2}}(\Gamma(t)))^d \rightarrow (H^1(\Omega(t)))^d$ to extend the boundary transformation Ψ_Γ and the boundary velocity $w_\Gamma \mathbf{n}$ to the volume transformations Ψ and \mathbf{w} ,

$$\Psi = \mathcal{E}(\Psi_\Gamma), \quad \implies \quad \mathbf{w} = \partial_t \Psi = \partial_t \mathcal{E}(\Psi_\Gamma) = \mathcal{E}(\partial_t \Psi_\Gamma) = \mathcal{E}(w_\Gamma \mathbf{n}). \quad (5)$$

3.1.3 Continuous subproblems

We write the ALE formulation for the continuous problem in terms of subproblems that are coupled in a time interval $(t_{n-1}, t_n]$. These subproblems are considered separately in the description of the discretization below:

1. Fix a time $t = t_*$. Given $\Psi(t_*)$ and $u(t_*)$, compute $w_\Gamma(t_*)$ as the solution to

$$w_\Gamma(t_*) = -\beta\kappa + \gamma(u(t_*) - u_{\text{ext}}) \quad \text{on } \Gamma(t_*). \quad (6a)$$

2. Fix a time $t = t_*$. Given $w_\Gamma(t_*)$, compute a volumetric velocity as a suitable extension $\mathbf{w}(t_*)$:

$$\mathbf{w}(t_*) = \mathcal{E}(w_\Gamma(t_*)\mathbf{n}). \quad (6b)$$

3. Given the mesh velocity $\mathbf{w}(t)$ in a time interval $(t_{n-1}, t_n]$ and the initial transformation at a time step Ψ_{init} , compute $\Psi(t)$, $t \in (t_{n-1}, t_n]$ as the solution to

$$\partial_t \Psi(t) = \mathbf{w}, \quad t \in (t_{n-1}, t_n], \quad \Psi(t_{n-1}) = \Psi_{\text{init}}. \quad (6c)$$

4. Given the domain $\Omega(t) = \Psi(t)(\hat{\Omega})$ in a time interval $(t_{n-1}, t_n]$ and initial concentration data for this time interval u_{init} , compute $u(t)$ as the solution to:

$$\begin{cases} \partial_t u - \alpha \Delta u = 0 & \text{in } \Omega(t), & t \in (t_{n-1}, t_n], \\ w_\Gamma u + \alpha \partial_{\mathbf{n}} u = 0 & \text{on } \Gamma(t), & t \in (t_{n-1}, t_n], \\ u(t_{n-1}) = u_{\text{init}} & \text{in } \Omega(t_{n-1}). \end{cases} \quad (6d)$$

3.2 Preliminaries, notation and decoupling scheme

In the discretization in this study we consider a simplicial triangulation \mathcal{T} defining the reference domain $\hat{\Omega}$. On \mathcal{T} we use the standard finite element space

$$\hat{U}_h := \{v \in C^0(\hat{\Omega}) \mid v|_T \in \mathcal{P}^k(T), \forall T \in \mathcal{T}\} \quad (7)$$

with $\mathcal{P}^k(T)$ the space of polynomials of degree at most k . Further, we define the vector valued space $\hat{\mathbf{U}}_h := (\hat{U}_h)^d$ and its trace space $\hat{\mathbf{U}}_h^\Gamma := \hat{\mathbf{U}}_h|_{\hat{\Gamma}}$ where $\hat{\Gamma} := \partial\hat{\Omega}$. For the concentration field we introduce the unknown $\hat{u}_h \in \hat{U}_h$ corresponding to a mapped function $u_h = \hat{u}_h \circ \Psi_h^{-1}$. Correspondingly, we have the unknown transformation field Ψ that is approximated by Ψ_h in $\hat{\mathbf{U}}_h$. The mesh velocity \mathbf{w} is approximated on the reference domain with $\hat{\mathbf{w}}_h \in \hat{\mathbf{U}}_h$ so that $\mathbf{w}_h = \hat{\mathbf{w}}_h \circ \Psi_h^{-1}$. The vector-valued boundary velocity $w_\Gamma \mathbf{n}$ is approximated with $\mathbf{w}_{\Gamma,h} = \hat{\mathbf{w}}_{\Gamma,h} \circ \Psi_h^{-1}$ with $\hat{\mathbf{w}}_{\Gamma,h}$ in the trace space $\hat{\mathbf{U}}_h^\Gamma$.

For the discretization in time we consider an equidistant decomposition of $(0, T]$ into N time intervals and define time steps $t_i := i\Delta t$ with $\Delta t = T/N$. We denote the discrete solutions at a time step t_i by u_h^i (\hat{u}_h^i), \mathbf{w}_h^i ($\hat{\mathbf{w}}_h^i$), $\mathbf{w}_{\Gamma,h}^i$ ($\hat{\mathbf{w}}_{\Gamma,h}^i$) and Ψ_h^i . Further, we introduce the notation Ω_h^i for the mapped domain $\Omega_h(t_i) := \Psi_h^i(\hat{\Omega})$ and accordingly define $\Gamma_h^i := \Psi_h^i(\hat{\Gamma})$.

In the remainder of this study, we consider a weakly coupled first order time integration scheme for the full discretization of the ALE formulation (6a)–(6d). One time step in the scheme consists of the successive application of the following steps:

1. Given Ψ_h^{n-1} , u_h^{n-1} compute $\hat{\mathbf{w}}_{\Gamma,h}^{n-1}$ approximating (6a), cf. Section 3.3.

2. Extend $\hat{\mathbf{w}}_{\Gamma,h}^{n-1}$ to $\hat{\Omega}$ resulting in $\hat{\mathbf{w}}_h^{n-1}$, cf. Section 3.4.

3. With Ψ_h^{n-1} and $\hat{\mathbf{w}}_h^{n-1}$ given, we approximate (6c) with an explicit Euler step:

$$\Psi_h^n = \Psi_h^{n-1} + \Delta t \hat{\mathbf{w}}_h^{n-1}. \quad (8)$$

4. Take Ψ_h^{n-1} and Ψ_h^n to approximate the domain evolution. With u_h^{n-1} compute an approximation u_h^n to (6d), cf. Section 3.5.

Below, for the application of integral transformations corresponding to a mapping Ψ , we make use of the following notations for the Jacobian \mathbf{F} , the Jacobian determinant J which is also the ratio of volume measure between preimage and image of Ψ , the normal to the mapped domain \mathbf{n} , the ratio of the surface measures J_Γ and the tangential projection onto the mapped domain \mathbf{P} :

$$\mathbf{F}(\Psi) := D\Psi, \quad (9a) \quad \mathbf{n}(\Psi) := \mathbf{F}^{-T}(\Psi) \hat{\mathbf{n}} \|\mathbf{F}^{-T}(\Psi) \hat{\mathbf{n}}\|^{-1}, \quad (9d)$$

$$J(\Psi) := \det(\mathbf{F}(\Psi)), \quad (9b) \quad \mathbf{P}(\Psi) := \mathbf{I} - \mathbf{n}(\Psi) \otimes \mathbf{n}^T(\Psi). \quad (9e)$$

$$J_\Gamma(\Psi) := \|\mathbf{F}^{-T}(\Psi) \hat{\mathbf{n}}\| J(\Psi), \quad (9c)$$

We notice that $\det(\mathbf{F}(\Psi))$ is positive as long as Ψ is sufficiently close to the identity, i.e. as long as the deformation of the domain does not get too large. We define \mathbf{F}^i as the Jacobian to Ψ_h^i , i.e. $\mathbf{F}^i = \mathbf{F}(\Psi_h^i)$ and define J^i , J_Γ^i , \mathbf{n}^i and \mathbf{P}^i accordingly.

3.3 Discretization of the boundary velocity

We want to approximate $w_\Gamma \mathbf{n}$ with w_Γ as in (6a) for $t_* = t_{n-1}$. Hence, we seek for an approximation $\hat{\mathbf{w}}_{\Gamma,h}^{n-1} \in \hat{\mathbf{U}}_\Gamma^h$ to

$$\hat{\mathbf{w}}_{\Gamma,h}^{n-1} \approx w_\Gamma \mathbf{n} = -\beta \kappa \mathbf{n} + \gamma(u(t_*) - u_{\text{ext}}) \mathbf{n} \quad \text{on } \Gamma_h^{n-1}. \quad (10)$$

Multiplying with a test function $\mathbf{s}_h = \hat{\mathbf{s}}_h \circ (\Psi_h^{n-1})^{-1}$, $\hat{\mathbf{s}}_h \in \hat{\mathbf{U}}_\Gamma^h$ and integrating over Γ_h^{n-1} yields

$$\int_{\Gamma_h^{n-1}} \mathbf{w}_{\Gamma,h}^{n-1} \cdot \mathbf{s}_h \, ds = -\beta \kappa_h^n(\mathbf{s}_h) + \gamma \int_{\Gamma_h^{n-1}} (u_h - u_{\text{ext}})(\mathbf{s}_h \cdot \mathbf{n}) \, ds, \quad (11)$$

where $\kappa_h^n(\mathbf{s}_h)$ is a discrete curvature linear form. To compute the mean curvature we make use of two main ideas from [4]. First, we use the Laplace-Beltrami characterization of the mean curvature, $-\kappa \mathbf{n} = \Delta_\Gamma \mathbf{id}$ in a weak formulation, to avoid the computation of second derivatives. This allows to make sense of a curvature even for polygonal boundaries. Secondly, it is well-known that an explicit treatment of the curvature in free boundary problems leads to (severe) time step restrictions. These can be circumvented using an implicit approximation of the curvature. Hence, we aim at computing the curvature at time t_n instead of t_{n-1} . As Γ_h^n is not known, we approximate

the identity operator on the boundary to time t_n by $\mathbf{x} + \Delta t \mathbf{w}_{\Gamma,h}^{n-1} = \mathbf{id}|_{\Gamma_h^{n-1}} + \Delta t \mathbf{w}_{\Gamma,h}^{n-1}$ which yields the discrete curvature linear form

$$\kappa_h^n(\mathbf{s}_h) := \int_{\Gamma_h^{n-1}} \nabla_\Gamma \mathbf{id} : \nabla_\Gamma \mathbf{s}_h \, ds + \Delta t \int_{\Gamma_h^{n-1}} \nabla_\Gamma \mathbf{w}_{\Gamma,h}^{n-1} : \nabla_\Gamma \mathbf{s}_h \, ds. \quad (12)$$

We notice that the superscript n at the linear form indicates that the curvature computation corresponds to time t_n . Hence, our discretization of (6a) is: Find $\mathbf{w}_{\Gamma,h}^{n-1} = \hat{\mathbf{w}}_{\Gamma,h}^{n-1} \circ (\boldsymbol{\Psi}_h^{n-1})^{-1}$ with $\hat{\mathbf{w}}_{\Gamma,h}^{n-1} \in \hat{\mathbf{U}}_\Gamma^h$, s.t. for all $\mathbf{s}_h = \hat{\mathbf{s}}_h \circ (\boldsymbol{\Psi}_h^{n-1})^{-1}$ with $\hat{\mathbf{s}}_h \in \hat{\mathbf{U}}_\Gamma^h$ there holds

$$\begin{aligned} \int_{\Gamma_h^{n-1}} \mathbf{w}_{\Gamma,h}^{n-1} \cdot \mathbf{s}_h \, ds + \beta \Delta t \int_{\Gamma_h^{n-1}} \nabla_\Gamma \mathbf{w}_{\Gamma,h}^{n-1} : \nabla_\Gamma \mathbf{s}_h \, ds \\ = -\beta \int_{\Gamma_h^{n-1}} \nabla_\Gamma \mathbf{id} : \nabla_\Gamma \mathbf{s}_h \, ds + \gamma \int_{\Gamma_h^{n-1}} (u_h - u_{\text{ext}})(\mathbf{s}_h \cdot \mathbf{n}) \, ds. \end{aligned} \quad (13)$$

Here, the tangential gradient acts on Γ_h^{n-1} , i.e. $\nabla_\Gamma \mathbf{id} = \mathbf{P} \cdot \nabla \mathbf{id} = \mathbf{P}$ where $\mathbf{P} = \mathbf{I} - \mathbf{n} \otimes \mathbf{n}^T$ is the tangential projection. With the notations from (9) and $\hat{\mathbf{n}}$ the outer normal to $\hat{\Omega}$, we can write this as an equation on $\hat{\Gamma}$: Find $\hat{\mathbf{w}}_{\Gamma,h}^{n-1} \in \hat{\mathbf{U}}_\Gamma^h$, s.t. for all $\hat{\mathbf{s}}_h \in \hat{\mathbf{U}}_\Gamma^h$ there holds

$$\begin{aligned} \int_{\hat{\Gamma}} J_\Gamma^{n-1} \hat{\mathbf{w}}_{\Gamma,h}^{n-1} \cdot \hat{\mathbf{s}}_h \, ds + \beta \Delta t \int_{\hat{\Gamma}} J_\Gamma^{n-1} (\mathbf{P} \cdot (\mathbf{F}^{n-1})^{-T} \cdot \nabla \hat{\mathbf{w}}_{\Gamma,h}^{n-1}) : ((\mathbf{F}^{n-1})^{-T} \nabla \hat{\mathbf{s}}_h) \, ds \\ = -\beta \int_{\hat{\Gamma}} J_\Gamma^{n-1} \mathbf{P} : (\mathbf{F}^{n-1})^{-T} \nabla_{\hat{\Gamma}} \hat{\mathbf{s}}_h \, ds + \gamma \int_{\hat{\Gamma}} J_\Gamma^{n-1} (\hat{u}_h - u_{\text{ext}}) \hat{\mathbf{s}}_h \cdot ((\mathbf{F}^{n-1})^{-T} \hat{\mathbf{n}}) \, ds. \end{aligned} \quad (14)$$

3.4 Extension of the boundary velocity

For a given boundary velocity $\hat{\mathbf{w}}_{\Gamma,h}^{n-1}$ (respectively $\mathbf{w}_{\Gamma,h}^{n-1}$) we seek for an extension $\hat{\mathbf{w}}_h^{n-1} = \mathcal{E}_h(\hat{\mathbf{w}}_{\Gamma,h}^{n-1}) \in \hat{\mathbf{U}}_h$ (respectively \mathbf{w}_h^{n-1}) and use the solution operator (in a standard FEM formulation) of an harmonic extension (on the reference domain), i.e. we define $\hat{\mathbf{w}}_h^{n-1} = \mathcal{E}_h(\hat{\mathbf{w}}_{\Gamma,h}^{n-1}) \in \hat{\mathbf{U}}_h$ as the solution to

$$-\text{div}[h_{\mathcal{T}}^{-1}(\nabla \hat{\mathbf{w}}_h^{n-1} + (\nabla \hat{\mathbf{w}}_h^{n-1})^T)] = 0 \quad \text{in } \hat{\Omega}, \quad (15a)$$

$$\hat{\mathbf{w}}_h^{n-1} = \hat{\mathbf{w}}_{\Gamma,h}^{n-1} \quad \text{on } \partial \hat{\Omega}, \quad (15b)$$

where $h_{\mathcal{T}}(\mathbf{x})$ is the locally constant grid function assigning to each $\mathbf{x} \in T \in \mathcal{T}$ the diameter of T .

Note that one easily finds more sophisticated choices of the extension operator in the literature which allow to provide more control on the shape regularity of deformed mesh for larger deformations, see e.g. [8, Section 5.1.2 and 5.1.3] and the references therein. In this study we consider only moderate deformations and take the liberty to consider only the simplified choice of an harmonic extension. We notice however that this restriction is not crucial for the applicability of the model order reduction considered below but simplifies the presentation as this extension operator is linear and parameter independent.

3.5 Conservative concentration update on a moving domain

We derive a time stepping procedure tailored to preserve the global solute mass. First, let us assume that a continuous mapping $\Psi : \hat{\Omega} \times (t_{n-1}, t_n] \rightarrow \mathbb{R}^d$ is known. To $\hat{v} \in \hat{U}_h$, we define the mapped function $v(\mathbf{x}, t) = \hat{v}(\Psi^{-1}(t)(\mathbf{x}))$ and apply Reynolds' transport theorem to the product uv where u is the exact solution to (6d). This gives

$$\begin{aligned} \frac{d}{dt} \int_{\Omega(t)} uv \, d\mathbf{x} &= \int_{\Omega(t)} \partial_t(uv) \, d\mathbf{x} + \int_{\partial\Omega} w_\Gamma uv \, d\mathbf{s} \\ &= \int_{\Omega(t)} \alpha \Delta uv - (\mathbf{w} \cdot \nabla v)u \, d\mathbf{x} + \int_{\partial\Omega} w_\Gamma uv \, d\mathbf{s} \\ &= \int_{\Omega(t)} -\alpha \nabla u \cdot \nabla v - (\mathbf{w} \cdot \nabla v)u \, d\mathbf{x}, \quad t \in (t_{n-1}, t_n]. \end{aligned} \quad (16)$$

where we made use of $\partial_t u = \alpha \Delta u$ (from (6d)), $\partial_t v = -\mathbf{w} \cdot \nabla v$ (chain rule) and the boundary conditions in (6d). Integration over $(t_{n-1}, t_n]$ then yields

$$\int_{\Omega(t_n)} uv \, d\mathbf{x} - \int_{\Omega(t_{n-1})} uv \, d\mathbf{x} = \int_{t_{n-1}}^{t_n} \int_{\Omega(t)} -\alpha \nabla u \cdot \nabla v - (\mathbf{w} \cdot \nabla v)u \, d\mathbf{x} \, dt. \quad (17)$$

By choosing $v = 1$ ($\hat{v} = 1$) we recover the conservation of the total solute concentration (2). To arrive at a discretization, we replace the time integral with the right hand side rule, the exact geometries with Ω_h^{n-1} and Ω_h^n and the solution u with the finite element approximations u_h^{n-1} and u_h^n , respectively, yielding the discrete problem:

Find $u_h^n = \hat{u}_h^n \circ (\Psi_h^n)^{-1}$ with $\hat{u}_h^n \in \hat{U}_h$ s.t. for all $v_h = \hat{v}_h \circ (\Psi_h^n)^{-1}$ with $\hat{v}_h \in \hat{U}_h$ there holds

$$\int_{\Omega_h^n} u_h^n v_h \, d\mathbf{x} + \Delta t \int_{\Omega_h^n} u_h^n \mathbf{w}_h^{n-1} \cdot \nabla v_h + \alpha \nabla u_h^n \cdot \nabla v_h \, d\mathbf{x} = \int_{\Omega_h^{n-1}} u_h^{n-1} v_h \, d\mathbf{x}. \quad (18)$$

Equivalently, we can formulate the discretization with respect to the reference domain $\hat{\Omega}$: Find $\hat{u}_h^n \in \hat{U}_h$, s.t. for all $\hat{v}_h \in \hat{U}_h$ there holds

$$\begin{aligned} \int_{\hat{\Omega}} J^n \hat{u}_h^n \hat{v}_h \, d\mathbf{x} + \Delta t \int_{\hat{\Omega}} J^n \hat{u}_h^n \hat{\mathbf{w}}_h^{n-1} \cdot ((\mathbf{F}^n)^{-T} \cdot \nabla \hat{v}_h) d\mathbf{x} \\ + \alpha \Delta t \int_{\hat{\Omega}} J^n ((\mathbf{F}^n)^{-T} \nabla \hat{u}_h^n) \cdot ((\mathbf{F}^n)^{-T} \nabla \hat{v}_h) \, d\mathbf{x} = \int_{\hat{\Omega}} J^{n-1} \hat{u}_h^{n-1} \hat{v}_h \, d\mathbf{x}. \end{aligned} \quad (19)$$

We notice that the conservation property (2) is preserved also on the discrete level.

4 Model order reduction

4.1 Parameterized full order model

As parameters to the problem (1) we consider the initial shape of the osmotic cell, the diffusivity α and the surface tension parameter β . We notice that with dimensional

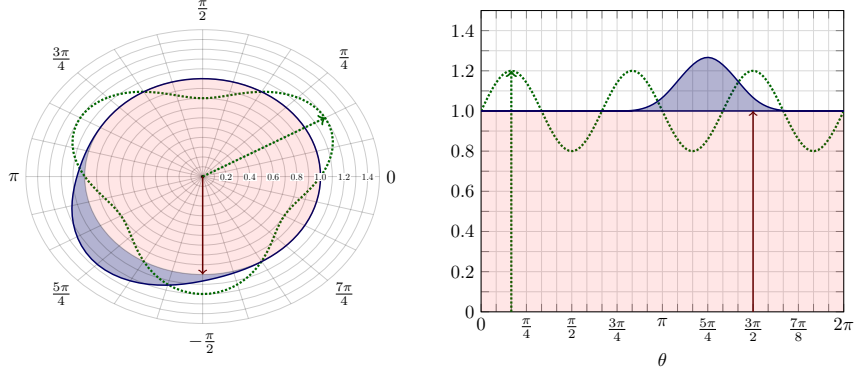


Figure 2: Sketch of possible initial shapes and corresponding graphs.

analysis one easily checks that — up to rescaling of time — γ is not an independent parameter in the model. Thus, in the following we assume γ to be constant. Possible other parameters are the initial and the exterior concentration $u_{\text{init}} = u(\cdot, 0)$, u_{ext} , which we will not consider in this study, however. For simplicity, we set $u_{\text{ext}} = 0$ in the sequel. Regarding the parameterization of the initial domain Ω_0 , we consider only initial shapes which are star-shaped and can be represented as a graph in normal direction, i.e.

$$\Gamma_0 = \{\mathbf{x} + r(\mathbf{x})\mathbf{n}(\mathbf{x}) \mid \mathbf{x} \in S_1(0)\}, \quad (20)$$

where S_1 is the unit sphere, \mathbf{n} is the unit outer normal to S_1 and r is C^1 -smooth on S_1 , cf. also Figure 2 for a sketch. As reference domain we choose the unit disk $\hat{\Omega} := D_2(0)$. For simplicity we assume that r is given as a linear combination of the form

$$r(\mathbf{x}) = \delta_1 r_1(\mathbf{x}) + \dots + \delta_L r_L(\mathbf{x}). \quad (21)$$

More general parameterizations could be considered using the empirical interpolation procedure described in Section 4.3. In total, the solution will depend on the parameter vector

$$\mu := (\alpha, \beta, \delta_1, \dots, \delta_L) \in \mathcal{P} \subset \mathbb{R}^{L+2}, \quad (22)$$

where \mathcal{P} is the set of admissible parameters. The dependence on μ will be signified by adding the subscript μ to the respective solution fields. The individual components of a parameter vector μ will be referred to as $\alpha_\mu, \beta_\mu, \delta_{1,\mu}, \dots, \delta_{L,\mu}$.

Summarizing the discretization derived in Section 3, the discrete solution fields $\hat{u}_{h,\mu}^n, \Psi_{h,\mu}^n$, $n = 0, \dots, N$ for $\mu \in \mathcal{P}$ are determined as follows:

As initial conditions we have

$$\hat{u}_{h,\mu}^0 = \mathcal{I}_h(u_{\text{init}}), \quad \Psi_{h,\mu}^0 = \mathbf{id} + \sum_{l=1}^L \delta_{l,\mu} \cdot \mathcal{E}_h(\mathcal{I}_{\Gamma,h}(r_l \mathbf{n})), \quad (23)$$

with $\mathcal{I}_h, \mathcal{I}_{\Gamma,h}$ denoting linear interpolation operators for $\hat{\mathbf{U}}_h, \hat{\mathbf{U}}_h^\Gamma$ and $\mathcal{E}_h(\hat{\boldsymbol{\psi}}_\Gamma)$ denoting the solution of the extension problem defined in Section 3.4 for given boundary data $\hat{\boldsymbol{\psi}}_\Gamma$.

We introduce some notation for bilinear and linear forms appearing in (14) and (19) which simplify the presentation of the model order reduction approach below: Problem (14) becomes

$$\begin{aligned} a_1(\hat{\mathbf{w}}_{\Gamma,h,\mu}^{n-1}, \hat{\mathbf{s}}_h; \boldsymbol{\Psi}_{h,\mu}^{n-1}) + \beta_\mu \Delta t \cdot a_2(\hat{\mathbf{w}}_{\Gamma,h,\mu}^{n-1}, \hat{\mathbf{s}}_h; \boldsymbol{\Psi}_{h,\mu}^{n-1}) \\ = -\beta_\mu \cdot l_1(\hat{\mathbf{s}}_h; \boldsymbol{\Psi}_{h,\mu}^{n-1}) + \gamma \cdot l_2(\hat{\mathbf{s}}_h; \boldsymbol{\Psi}_{h,\mu}^{n-1}, \hat{u}_{h,\mu}^{n-1}) \quad \forall \hat{\mathbf{s}}_h \in \hat{\mathbf{U}}_h^\Gamma. \end{aligned} \quad (24a)$$

For the update of the transformation field we have

$$\hat{\mathbf{w}}_{h,\mu}^{n-1} = \mathcal{E}_h(\hat{\mathbf{w}}_{\Gamma,h,\mu}^{n-1}), \quad \boldsymbol{\Psi}_{h,\mu}^n = \boldsymbol{\Psi}_{h,\mu}^{n-1} + \Delta t \hat{\mathbf{w}}_{h,\mu}^{n-1} \quad (24b)$$

where \mathcal{E}_h is the extension operator from (15). The concentration update, cf. (19), reads as

$$\begin{aligned} a_3(\hat{u}_{h,\mu}^n, \hat{v}_h; \boldsymbol{\Psi}_{h,\mu}^n) + \Delta t \cdot a_4(\hat{u}_{h,\mu}^n, \hat{v}_h; \boldsymbol{\Psi}_{h,\mu}^n, \hat{\mathbf{w}}_{h,\mu}^{n-1}) \\ + \alpha_\mu \Delta t \cdot a_5(\hat{u}_{h,\mu}^n, \hat{v}_h; \boldsymbol{\Psi}_{h,\mu}^n) = a_3(\hat{u}_{h,\mu}^{n-1}, \hat{v}_h; \boldsymbol{\Psi}_{h,\mu}^{n-1}) \quad \forall \hat{v}_h \in \hat{U}_h. \end{aligned} \quad (24c)$$

In these equation systems, $a_1, a_2 : H^{\frac{1}{2}}(\hat{\Gamma})^d \times H^{\frac{1}{2}}(\hat{\Gamma})^d \rightarrow \mathbb{R}$, $l_1, l_2 \in (H^{\frac{1}{2}}(\hat{\Gamma})^d)'$, $a_3, a_5, a_4 : H^{\hat{\Omega}} \times H^{\hat{\Omega}} \rightarrow \mathbb{R}$, are bilinear and linear forms given by

$$a_1(\hat{q}, \hat{\mathbf{s}}; \hat{\boldsymbol{\psi}}) := \int_{\hat{\Gamma}} c_1(\hat{\boldsymbol{\psi}}) \hat{q} \cdot \hat{\mathbf{s}} \, d\mathbf{s}, \quad a_5(\hat{u}, \hat{v}; \hat{\boldsymbol{\psi}}) := \int_{\hat{\Omega}} c_5(\hat{\boldsymbol{\psi}}) \nabla \hat{u} \cdot \nabla \hat{v} \, d\mathbf{x}, \quad (25a)$$

$$a_2(\hat{q}, \hat{\mathbf{s}}; \hat{\boldsymbol{\psi}}) := \int_{\hat{\Gamma}} c_2(\hat{\boldsymbol{\psi}}) \cdot \nabla_{\hat{\Gamma}} \hat{q} : \nabla_{\hat{\Gamma}} \hat{\mathbf{s}} \, d\mathbf{s}, \quad l_1(\hat{\mathbf{s}}; \hat{\boldsymbol{\psi}}) := \int_{\hat{\Gamma}} c_6(\hat{\boldsymbol{\psi}}) : \nabla_{\hat{\Gamma}} \hat{\mathbf{s}} \, d\mathbf{s}, \quad (25b)$$

$$a_3(\hat{u}, \hat{v}; \hat{\boldsymbol{\psi}}) := \int_{\hat{\Omega}} c_3(\hat{\boldsymbol{\psi}}) \hat{u} \, \hat{v} \, d\mathbf{x}, \quad l_2(\hat{\mathbf{s}}; \hat{\boldsymbol{\psi}}, \hat{\varphi}) := \int_{\hat{\Gamma}} c_7(\hat{\boldsymbol{\psi}}, \hat{\varphi}) \cdot \hat{\mathbf{s}} \, d\mathbf{s}, \quad (25c)$$

$$a_4(\hat{u}, \hat{v}; \hat{\boldsymbol{\psi}}, \hat{\boldsymbol{\eta}}) := \int_{\hat{\Omega}} c_4(\hat{\boldsymbol{\psi}}, \hat{\boldsymbol{\eta}}) \hat{u} \cdot \nabla \hat{v} \, d\mathbf{x}, \quad (25d)$$

with coefficient functions

$$c_1(\hat{\boldsymbol{\psi}}) := J_\Gamma(\hat{\boldsymbol{\psi}}), \quad c_5(\hat{\boldsymbol{\psi}}) := J(\hat{\boldsymbol{\psi}}) \mathbf{F}^{-1}(\hat{\boldsymbol{\psi}}) \mathbf{F}^{-T}(\hat{\boldsymbol{\psi}}), \quad (26a)$$

$$c_2(\hat{\boldsymbol{\psi}}) := J_\Gamma(\hat{\boldsymbol{\psi}}) \mathbf{F}^{-1}(\hat{\boldsymbol{\psi}}) \cdot \mathbf{P}(\hat{\boldsymbol{\psi}}) \cdot \mathbf{F}^{-T}(\hat{\boldsymbol{\psi}}), \quad c_6(\hat{\boldsymbol{\psi}}) := J_\Gamma(\hat{\boldsymbol{\psi}}) \mathbf{F}^{-1}(\hat{\boldsymbol{\psi}}) \cdot \mathbf{P}(\hat{\boldsymbol{\psi}}), \quad (26b)$$

$$c_3(\hat{\boldsymbol{\psi}}) := J(\hat{\boldsymbol{\psi}}), \quad c_7(\hat{\boldsymbol{\psi}}, \hat{\varphi}) := J_\Gamma(\hat{\boldsymbol{\psi}}) \mathbf{F}^{-T}(\hat{\boldsymbol{\psi}}) \cdot \hat{\mathbf{n}} \cdot \hat{\varphi}, \quad (26c)$$

$$c_4(\hat{\boldsymbol{\psi}}, \hat{\boldsymbol{\eta}}) := J(\hat{\boldsymbol{\psi}}) \mathbf{F}^{-1}(\hat{\boldsymbol{\psi}}) \cdot \hat{\boldsymbol{\eta}}, \quad (26d)$$

where we made use of the notation from (9).

4.2 Reduced basis approximation

We construct a ROM for (23), (24) via Galerkin projection onto reduced order approximation spaces $\hat{\mathbf{U}}_r^\Gamma \subset \hat{\mathbf{U}}_h^\Gamma$, $\hat{\mathbf{U}}_r \subset \hat{\mathbf{U}}_h$, $\hat{U}_r \subset \hat{U}_h$ for the solution fields $\hat{\mathbf{w}}_{\Gamma,h,\mu}^n$, $\boldsymbol{\Psi}_{h,\mu}^n$ and $\hat{u}_{h,\mu}^n$, $n = 0, \dots, N$.

Many different strategies have been discussed in the literature for constructing low-dimensional reduced approximation spaces from solution snapshots of the full order model (23), (24). In this study we choose a basic proper orthogonal decomposition (POD, [31]) approach:

We assume that an appropriate finite set of training parameters $\mathcal{S}_{train} \subset \mathcal{P}$ has been chosen and compute the snapshot sets

$$\mathbf{M}_\Gamma := \{\hat{\mathbf{w}}_{\Gamma,h,\mu}^n \mid \mu \in \mathcal{S}_{train}, 0 \leq n \leq N\}, \quad (27a)$$

$$\mathbf{M}_\Psi := \{\Psi_{h,\mu}^n - \mathbf{id} \mid \mu \in \mathcal{S}_{train}, 0 \leq n \leq N\}, \quad (27b)$$

$$M_u := \{\hat{u}_{h,\mu}^n \mid \mu \in \mathcal{S}_{train}, 0 \leq n \leq N\}, \quad (27c)$$

of the solution time trajectories of (23), (24) for the parameter vectors $\mu \in \mathcal{S}_{train}$. The affine shift in the definition of \mathbf{M}_Ψ is introduced in accordance with the implementation used in Section 5, where the mesh deformations $\Psi_{h,\mu}^k - \mathbf{id}$ are used as solution variable.

The reduced approximation spaces $\hat{\mathbf{U}}_\Gamma^r$, $\hat{\mathbf{U}}_r$, \hat{U}_r are now obtained from a POD of \mathbf{M}_Γ , \mathbf{M}_Ψ , M_u , respectively, for a given relative truncation error tolerance ε_{rb} : The reduced spaces are spanned by the first K left-singular vectors of the linear mapping Φ_* sending the k -th canonical basis vector of $\mathbb{R}^{|M_*|}$ to s_k where $\{s_1, \dots, s_{|M_*|}\}$ is an arbitrary enumeration of the snapshot set. The singular value decomposition is computed w.r.t. the $H^1(\hat{\Omega})$ -inner product on \hat{U}_h , the $(H^1(\hat{\Omega}))^d$ -inner product on $\hat{\mathbf{U}}_h$, resp. the $(L^2(\hat{\Gamma}))^d$ -inner product on $\hat{\mathbf{U}}_h^r$. The truncation rank K is determined as the minimal K s.t. $\sigma_{K+1}(\Phi_*)/\sigma_1(\Phi_*) < \varepsilon_{rb}$, where $\sigma_k(\Phi_*)$ denotes the k -th singular value of Φ_* .

Denoting the $H^1(\hat{\Omega})$ -orthogonal projection of \hat{U}_h onto \hat{U}_r by P_r and the $(H^1(\hat{\Omega}))^d$ -orthogonal projection of $\hat{\mathbf{U}}_h$ onto $\hat{\mathbf{U}}_r$ by \mathbf{P}_r , the reduced order model is given as follows: For $\mu \in \mathcal{P}$, find $\hat{u}_{r,\mu}^n \in \hat{U}_r$, $\Psi_{r,\mu}^n \in \mathbf{id} + \hat{\mathbf{U}}_r$, $0 \leq n \leq N$ with initial data

$$\hat{u}_{r,\mu}^0 = P_r(\mathcal{I}_h(u_{init})), \quad \Psi_{r,\mu}^0 = \mathbf{id} + \sum_{l=1}^L \delta_l \cdot \mathbf{P}_r(\mathcal{E}_h(\mathcal{I}_{\Gamma,h}(r_l))), \quad (28)$$

with the boundary velocity $\hat{\mathbf{w}}_{\Gamma,r,\mu}^{n-1} \in \hat{\mathbf{U}}_\Gamma^r$ given by

$$\begin{aligned} a_1(\hat{\mathbf{w}}_{\Gamma,r,\mu}^{n-1}, \hat{\mathbf{s}}_r; \Psi_{r,\mu}^{n-1}) + \beta_\mu \Delta t \cdot a_2(\hat{\mathbf{w}}_{\Gamma,r,\mu}^{n-1}, \hat{\mathbf{s}}_r; \Psi_{r,\mu}^{n-1}) \\ = -\beta_\mu \cdot l_1(\hat{\mathbf{s}}_r; \Psi_{r,\mu}^{n-1}) + \gamma \cdot l_2(\hat{\mathbf{s}}_r; \Psi_{r,\mu}^{n-1}, \hat{u}_{r,\mu}^{n-1}) \quad \forall \hat{\mathbf{s}}_r \in \hat{\mathbf{U}}_\Gamma^r, \end{aligned} \quad (29a)$$

with the transformation field update given by

$$\hat{\mathbf{w}}_{r,\mu}^{n-1} = \mathbf{P}_r(\mathcal{E}_h(\hat{\mathbf{w}}_{\Gamma,r,\mu}^{n-1})), \quad \Psi_{r,\mu}^n = \Psi_{r,\mu}^{n-1} + \Delta t \hat{\mathbf{w}}_{r,\mu}^{n-1} \quad (29b)$$

and with the concentration field update given by

$$\begin{aligned} a_3(\hat{u}_{r,\mu}^n, \hat{v}_r; \Psi_{r,\mu}^n) + \Delta t \cdot a_4(\hat{u}_{r,\mu}^n, \hat{v}_r; \Psi_{r,\mu}^n, \hat{\mathbf{w}}_{r,\mu}^{n-1}) \\ + \alpha_\mu \Delta t \cdot a_5(\hat{u}_{r,\mu}^n, \hat{v}_r; \Psi_{r,\mu}^n) = a_3(\hat{u}_{r,\mu}^{n-1}, \hat{v}_r; \Psi_{r,\mu}^{n-1}) \quad \forall \hat{v}_r \in \hat{U}_r. \end{aligned} \quad (29c)$$

In order to solve (28), (29), we choose orthonormal bases of \hat{U}_r , $\hat{\mathbf{U}}_r$, $\hat{\mathbf{U}}_\Gamma^r$. We assemble the matrix of the linear operator $\mathbf{P}_r \circ \mathcal{E}_h$ with respect to these bases, as well

as the coefficient vectors of $P_r(\mathcal{I}_h(u_{init}))$, and $\mathbf{P}_r(\mathcal{E}_h(\mathcal{I}_{\Gamma,h}(r_l)))$ for the initial condition (28). In each time step, we then assemble the matrices and vectors of all bilinear forms a_* and linear forms l_* appearing in (29a), (29c). After that, the effort related to the computation of the basis coefficients of $\hat{u}_{r,\mu}^n$, $\Psi_{r,\mu}^n$ is

$$\mathcal{O}((\dim \hat{\mathbf{U}}_r^\Gamma)^3 + \dim \hat{\mathbf{U}}_r \cdot \dim \hat{\mathbf{U}}_r^\Gamma + (\dim \hat{U}_r)^3), \quad (30)$$

where the summands correspond to the solution of (29a), (29b) and (29c). However, due to the dependence of the bilinear / linear forms on $\Psi_{r,\mu}^n$, $\hat{\mathbf{w}}_{r,\mu}^n$, $\hat{u}_{r,\mu}^n$, the matrix assembly has to be carried out in each time step, requiring substantial computational effort proportional to $\dim \hat{U}_h$. In the following section we use empirical interpolation to overcome this issue.

4.3 Online efficient simulation via empirical interpolation

In order to achieve a fast assembly of (29a), (29c) we use empirical interpolation [5] to approximate the coefficient functions (26) by linear combinations

$$c_i(\hat{\psi}) \approx \sum_{m=1}^{M_i} \theta_i^m(\hat{\psi}) c_i^m, \quad \theta_i^m(\hat{\psi}) = [c_i(\hat{\psi})(\mathbf{x}_i^m)]_{k_i^m}, \quad i \neq 4, 7 \quad (31a)$$

$$c_4(\hat{\psi}, \hat{\eta}) \approx \sum_{m=1}^{M_4} \theta_4^m(\hat{\psi}, \hat{\eta}) c_4^m, \quad \theta_4^m(\hat{\psi}, \hat{\eta}) = [c_4(\hat{\psi}, \hat{\eta})(\mathbf{x}_4^m)]_{k_4^m}, \quad (31b)$$

$$c_7(\hat{\psi}, \hat{\phi}) \approx \sum_{m=1}^{M_7} \theta_7^m(\hat{\psi}, \hat{\phi}) c_7^m, \quad \theta_7^m(\hat{\psi}, \hat{\phi}) = [c_7(\hat{\psi}, \hat{\phi})(\mathbf{x}_7^m)]_{k_7^m}, \quad (31c)$$

where for $i = 1, \dots, 7$ the functions c_i^m no longer depend on $\hat{\psi}$, $\hat{\eta}$ or $\hat{\phi}$, $\mathbf{x}_i^m \in \hat{\Omega}$ (resp. $\mathbf{x}_i^m \in \hat{\Gamma}$) are interpolation points for c_i and k_i^m are vector indices resp. matrix indices selecting a scalar component of the evaluation of c_i at \mathbf{x}_i^m .

Defining the linear and bilinear forms

$$a_1^m(\hat{q}, \hat{\mathbf{s}}) := \int_{\hat{\Gamma}} c_1^m \hat{q} \cdot \hat{\mathbf{s}} \, d\mathbf{s}, \quad a_5^m(\hat{u}, \hat{v}) := \int_{\hat{\Omega}} c_5^m \nabla \hat{u} \cdot \nabla \hat{v} \, d\mathbf{x}, \quad (32a)$$

$$a_2^m(\hat{q}, \hat{\mathbf{s}}) := \int_{\hat{\Gamma}} a_2^m \cdot \nabla_{\hat{\Gamma}} \hat{q} : \nabla_{\hat{\Gamma}} \hat{\mathbf{s}} \, d\mathbf{s}, \quad l_1^m(\hat{\mathbf{s}}) := \int_{\hat{\Gamma}} c_6^m : \nabla_{\hat{\Gamma}} \hat{\mathbf{s}} \, d\mathbf{s}, \quad (32b)$$

$$a_3^m(\hat{u}, \hat{v}) := \int_{\hat{\Omega}} c_3^m \hat{u} \hat{v} \, d\mathbf{x}, \quad l_2^m(\hat{\mathbf{s}}) := \int_{\hat{\Gamma}} c_7^m \cdot \hat{\mathbf{s}} \, d\mathbf{s}, \quad (32c)$$

$$a_4^m(\hat{u}, \hat{v}) := \int_{\hat{\Omega}} c_4^m \hat{u} \cdot \nabla \hat{v} \, d\mathbf{x}, \quad (32d)$$

we obtain approximations $a_i \approx \sum_{m=1}^{M_i} \theta_i^m \cdot a_i^m$ and $l_i \approx \sum_{m=1}^{M_i} \theta_{i+5}^m \cdot l_i^m$ yielding the

update equations

$$\begin{aligned} & \sum_{m=1}^{M_1} \theta_1^m(\Psi_{r,\mu}^{n-1}) \cdot a_1^m(\hat{\mathbf{w}}_{\Gamma,r,\mu}^{n-1}, \hat{\mathbf{s}}_r) + \beta_\mu \Delta t \cdot \sum_{m=1}^{M_2} \theta_2^m(\Psi_{r,\mu}^{n-1}) \cdot a_2^m(\hat{\mathbf{w}}_{\Gamma,r,\mu}^{n-1}, \hat{\mathbf{s}}_r) \\ &= -\beta_\mu \cdot \sum_{m=1}^{M_6} \theta_6^m(\Psi_{r,\mu}^{n-1}) \cdot l_1^m(\hat{\mathbf{s}}_r) + \gamma \cdot \sum_{m=1}^{M_7} \theta_7^m(\Psi_{r,\mu}^{n-1}, \hat{u}_{r,\mu}^{n-1}) \cdot l_7^m(\hat{\mathbf{s}}_r) \quad \forall \hat{\mathbf{s}}_r \in \hat{\mathbf{U}}_r^\Gamma, \end{aligned} \quad (33a)$$

and

$$\begin{aligned} & \sum_{m=1}^{M_3} \theta_3^m(\Psi_{r,\mu}^n) \cdot a_3^m(\hat{u}_{r,\mu}^n, \hat{v}_r) + \Delta t \cdot \sum_{m=1}^{M_4} \theta_4^m(\Psi_{r,\mu}^n, \hat{\mathbf{w}}_{r,\mu}^{n-1}) \cdot a_4^m(\hat{u}_{r,\mu}^n, \hat{v}_r) \\ &+ \alpha_\mu \Delta t \cdot \sum_{m=1}^{M_5} \theta_5^m(\Psi_{r,\mu}^n) \cdot a_5^m(\hat{u}_{r,\mu}^n, \hat{v}_r) = \sum_{m=1}^{M_3} \theta_3^m(\Psi_{r,\mu}^{n-1}) \cdot a_3^m(\hat{u}_{r,\mu}^{n-1}, \hat{v}_r) \quad \forall \hat{v}_r \in \hat{U}_r. \end{aligned} \quad (33b)$$

After pre-assembly of the matrices of a_i^m and coefficient vectors of l_i^m , the effort for the assembly of the equation systems (33a), (33b) for an arbitrary $\mu \in \mathcal{P}$ is of order

$$\mathcal{O}(M_{1,2} \cdot (\dim \hat{\mathbf{U}}_r^\Gamma)^2 + M_{6,7} \cdot \dim \hat{\mathbf{U}}_r^\Gamma + M_{3,4,5} \cdot (\dim \hat{U}_r)^2), \quad (34)$$

with $M_{1,2} := M_1 + M_2$, $M_{3,4,5} := M_3 + M_4 + M_5$ and $M_{6,7} := M_6 + M_7$.

Computation of the interpolation data. We consider training sets of function evaluations

$$\begin{aligned} \mathcal{C}_i &:= \{[c_i(\Psi_{h,\mu}^n)(\mathbf{x}_j)]_j \mid \mu \in \mathcal{S}_{train}, 0 \leq n \leq N, 1 \leq j \leq |\mathcal{X}_i|\} \subset \ell^\infty(\mathcal{X}_i)^{d_i}, \quad i \neq 4, 7, \\ \mathcal{C}_4 &:= \{[c_4(\Psi_{h,\mu}^n, \hat{\mathbf{w}}_{r,\mu}^{n-1})(\mathbf{x}_j)]_j \mid \mu \in \mathcal{S}_{train}, 0 \leq n \leq N, 1 \leq j \leq |\mathcal{X}_i|\} \subset \ell^\infty(\mathcal{X}_i)^{d_4}, \\ \mathcal{C}_7 &:= \{[c_7(\Psi_{h,\mu}^n, \hat{u}_{h,\mu}^n)(\mathbf{x}_j)]_j \mid \mu \in \mathcal{S}_{train}, 0 \leq n \leq N, 1 \leq j \leq |\mathcal{X}_i|\} \subset \ell^\infty(\mathcal{X}_i)^{d_7}, \end{aligned} \quad (35)$$

where $\mathcal{X}_i = \{\mathbf{x}_1, \dots, \mathbf{x}_{|\mathcal{X}_i|}\}$ is an appropriate finite subset of $\hat{\Gamma}$ ($i = 1, 2, 6, 7$) resp. $\hat{\Omega}$ ($i = 3, 4, 5$) and d_i corresponds to the shape of the values of c_i , i.e. $d_1 = d_3 = 1$, $d_4 = d_7 = d$ and $d_2 = d_5 = d_6 = d^2$. Using the \mathcal{C}_i as input for the greedy algorithm from [5], interpreting tensor fields in $\ell^\infty(\mathcal{X}_i)^{d_i} \cong \ell^\infty(\dot{\bigcup}_{k=1}^{d_i} \mathcal{X}_i)$ as scalar functions, we obtain the desired interpolation basis functions $c_i^m \in \text{span}(\mathcal{C}_i)$ and interpolation points $\mathbf{x}_i^m \in \mathcal{X}_i$, $1 \leq k_i^m \leq d_i$, which approximate all elements of \mathcal{C}_i with a relative $\ell^\infty(\mathcal{X}_i)^{d_i}$ -error smaller than a prescribed tolerance ε_{ei} .

Note that for the evaluation of the bilinear forms a_i^m and the linear forms l_i^m , knowledge of the corresponding coefficient function c_i^m is only required at the finitely many quadrature points used in the discretization scheme. Hence, it is sufficient to choose \mathcal{X}_i as the set of all these quadrature points. Also note that our approach differs from [3] in which each coefficient tensor component is interpolated separately, whereas we perform a single interpolation of the full tensor field using tensor-valued interpolation basis functions and scalar components of the tensor at given $\mathbf{x} \in \mathcal{X}_i$ as interpolation

points. Since separate empirical interpolation of the tensor field components will in general select different interpolation points $\mathbf{x} \in \mathcal{X}_i$ for the individual components, we expect our approach to be more efficient in general (i.e. require less coefficient tensor evaluations).

Minimally intrusive implementation of empirical interpolation. In many cases it is technically difficult to replace in the PDE solver's matrix assembly code the analytically defined coefficient functions c_i by a vector of function evaluations c_i^m at the given quadrature points. In the numerical example in Section 5 we have used the following less intrusive approach to implement the empirical interpolation procedure, which in addition does not require knowledge of the exact quadrature points used by the assembly routine:

Noting that $c_i^m \in \text{span}(\mathcal{C}_i)$, we can represent c_i^m , $i = 1, 2, 3, 5$, as

$$c_i^m = \sum_{\mu \in \mathcal{S}_{train}} \sum_{n=1}^N \gamma_{i,\mu}^{m,n} \cdot [c_i(\Psi_{h,\mu}^n)(\mathbf{x}_j)]_j, \quad (36)$$

where the linear coefficients $\gamma_{i,\mu}^{m,n}$ can be directly obtained from the execution of the greedy algorithm. Using this representation, it immediately follows that

$$a_i^m(\cdot, \cdot) = \sum_{\mu \in \mathcal{S}_{train}} \sum_{n=1}^N \gamma_{i,\mu}^{m,n} \cdot a_i(\cdot, \cdot; \Psi_{h,\mu}^n). \quad (37)$$

Since the matrices $a_i(\cdot, \cdot; \Psi_{h,\mu}^n)$ have already been computed by the PDE solver, we can easily assemble the matrix of a_i^m using this formula. The same argument applies to a_4 , l_1^m , l_2^m .

4.4 Global mass conservation

As discussed in Section 3.5, choosing the test function $\hat{v}_h \equiv 1$ in the concentration update equation (19) shows that the total mass $\int_{\Omega_h^n} u_h^n d\mathbf{x}$ is conserved by the discretization scheme, i.e. $\int_{\Omega_h^n} u_h^n d\mathbf{x} = \int_{\Omega_h^0} u_h^0 d\mathbf{x}$ for all $0 \leq n \leq N$. By including the constant functions in the reduced concentration space \hat{U}_r ,

$$1 \in \hat{U}_r, \quad (38)$$

the same argument can be applied to the reduced concentration field given by (29c):

$$\begin{aligned} \int_{\Omega_{r,\mu}^n} u_{r,\mu}^n d\mathbf{x} &= a_3(\hat{u}_{r,\mu}^n, 1; \Psi_{r,\mu}^n) + \Delta t \cdot \underbrace{a_4(\hat{u}_{r,\mu}^n, 1; \Psi_{h,\mu}^n, \hat{\mathbf{w}}_{r,\mu}^{n-1})}_{=0} + \alpha_\mu \Delta t \cdot \underbrace{a_5(\hat{u}_{r,\mu}^n, 1; \Psi_{r,\mu}^n)}_{=0} \\ &= a_3(\hat{u}_{r,\mu}^{n-1}, 1; \Psi_{r,\mu}^{n-1}) = \int_{\Omega_{r,\mu}^{n-1}} u_{r,\mu}^{n-1} d\mathbf{x}. \end{aligned} \quad (39)$$

Here, $\Omega_{r,\mu}^n := \boldsymbol{\Psi}_{r,\mu}^n(\hat{\Omega})$ is the deformed domain at time step n given by the reduced transformation field $\boldsymbol{\Psi}_{r,\mu}^n$ and $u_{r,\mu}^n := \hat{u}_{r,\mu}^n \circ (\boldsymbol{\Psi}_{r,\mu}^n)^{-1}$ the reduced concentration field on this domain.

Note, however, that the argument in (39) is no longer valid when replacing the bilinear forms a_3, a_4, a_5 by their empirical interpolants (33b): While it still holds that

$$\sum_{m=1}^{M_4} \theta_4^m(\boldsymbol{\Psi}_{r,\mu}^n, \hat{\mathbf{w}}_{r,\mu}^{n-1}) \cdot \underbrace{a_4^m(\hat{u}_{r,\mu}^n, 1)}_{=0} = \sum_{m=1}^{M_5} \theta_5^m(\boldsymbol{\Psi}_{r,\mu}^n) \cdot \underbrace{a_5^m(\hat{u}_{r,\mu}^n, 1)}_{=0} = 0, \quad (40)$$

the total mass at time step n is only approximately given by the empirical interpolant of a_3 :

$$\int_{\Omega_{r,\mu}^n} u_{r,\mu}^n d\mathbf{x} \approx \sum_{m=1}^{M_3} \theta_3^m(\boldsymbol{\Psi}_{r,\mu}^n) \cdot a_3^m(\hat{u}_{r,\mu}^n, 1). \quad (41)$$

One way to recover exact mass conservation in the ROM is to apply the empirical interpolation procedure only to the coefficient functions of a_4, a_5 , whereas $a_3(\cdot, \cdot; \boldsymbol{\Psi}_{r,\mu}^n)$ is evaluated exactly. For $d = 2$, we can evaluate a_3 as

$$a_3(\cdot, \cdot, \boldsymbol{\Psi}_{r,\mu}^n) = \bar{a}_3(\cdot, \cdot, \boldsymbol{\Psi}_{r,\mu}^n, \boldsymbol{\Psi}_{r,\mu}^n), \quad (42)$$

where \bar{a}_3 is the 4-tensor given by

$$\bar{a}_3(\hat{u}, \hat{v}, \hat{\boldsymbol{\psi}}, \hat{\boldsymbol{\eta}}) = \int_{\hat{\Omega}} (\partial_1 \hat{\boldsymbol{\psi}}_1 \cdot \partial_2 \hat{\boldsymbol{\eta}}_2 - \partial_1 \hat{\boldsymbol{\psi}}_2 \cdot \partial_2 \hat{\boldsymbol{\eta}}_1) \cdot \hat{u} \cdot \hat{v} d\mathbf{x}. \quad (43)$$

The effort to assemble the matrix of $a_3(\cdot, \cdot; \boldsymbol{\Psi}_{r,\mu}^n)$ from the coefficients of \bar{a}_3 w.r.t. a basis of \hat{U}_r is of order $\mathcal{O}((\dim \hat{U}_r)^2 \cdot (\dim \hat{\mathbf{U}}_r)^2)$. Although highly efficient implementations for this operation are available, the higher computational complexity in comparison to (30), (34) will lead to dominating runtime costs for large reduced space dimensions. In three spatial dimensions ($d = 3$), the matrix of a_3 can be assembled exactly by the same argument with a computational effort of $\mathcal{O}((\dim \hat{U}_r)^2 \cdot (\dim \hat{\mathbf{U}}_r)^3)$. We expect this to be non-favorable, even for relatively small dimensions of \hat{U}_r . However, to ensure mass conservation, only the functional $a_3(\cdot, 1; \boldsymbol{\Psi}_{r,\mu}^n)$ needs to be known exactly, the matrix of which can be computed by the same argument with a reduced effort of $\mathcal{O}((\dim \hat{U}_r) \cdot (\dim \hat{\mathbf{U}}_r)^d)$.

Thus, choosing a basis $\hat{\varphi}_i$, $1 \leq i \leq \dim \hat{U}_r$ for \hat{U}_r such that $\varphi_1 = 1$, we define the reduced bilinear form $\tilde{a}_3(\hat{u}_r, \hat{v}_r; \hat{\boldsymbol{\psi}}_r)$ on \hat{U}_r by

$$\tilde{a}_3(\hat{u}_r, \hat{\varphi}_i; \hat{\boldsymbol{\psi}}_r) := \begin{cases} a_3(\hat{u}_r, 1; \hat{\boldsymbol{\psi}}_r) & i = 1 \\ \sum_{m=1}^{M_3} \theta_3^m(\hat{\boldsymbol{\psi}}_r) \cdot a_3^m(\hat{u}_r, \hat{\varphi}_i) & 2 \leq i \leq \dim \hat{U}_r, \end{cases} \quad (44)$$

and use as exactly mass conservative concentration update equation:

$$\begin{aligned} \tilde{a}_3(\hat{u}_{r,\mu}^n, \hat{v}_r; \boldsymbol{\Psi}_{r,\mu}^n) + \Delta t \cdot \sum_{m=1}^{M_4} \theta_4^m(\boldsymbol{\Psi}_{r,\mu}^n, \hat{\mathbf{w}}_{r,\mu}^{n-1}) \cdot a_4^m(\hat{u}_{r,\mu}^n, \hat{v}_r) \\ + \alpha_\mu \Delta t \cdot \sum_{m=1}^{M_5} \theta_5^m(\boldsymbol{\Psi}_{r,\mu}^n) \cdot a_5^m(\hat{u}_{r,\mu}^n, \hat{v}_r) = \tilde{a}_3(\hat{u}_{r,\mu}^{n-1}, \hat{v}_r; \boldsymbol{\Psi}_{r,\mu}^{n-1}) \quad \forall \hat{v}_r \in \hat{U}_r. \end{aligned} \quad (45)$$

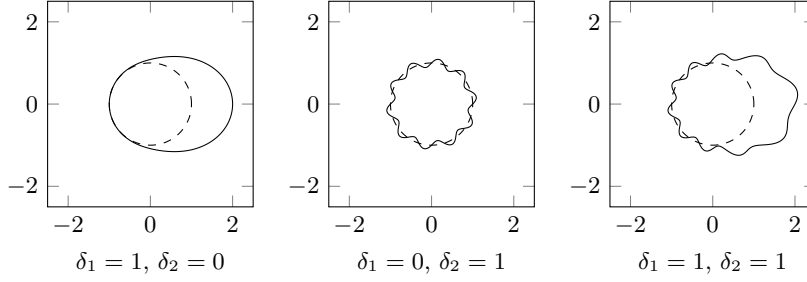


Figure 3: Initial boundary I_0 for different parameter combinations δ_1, δ_2 in the numerical experiment (solid line).

In total, this equation system can then be assembled with an effort of

$$\mathcal{O}(M_{3,4,5} \cdot (\dim \hat{U}_r)^2 + (\dim \hat{U}_r) \cdot (\dim \hat{\mathbf{U}}_r)^d). \quad (46)$$

5 Numerical experiments

As a test for the developed reduced order modeling workflow we consider the parameterized model from Section 4.1 in two spatial dimensions and a two-dimensional parameterization ($L = 2$) of the initial boundary I_0 given by

$$r_1(\mathbf{x}) := e^{-\theta(\mathbf{x})^2} \cdot \mathbf{x}, \quad \theta(\mathbf{x}) := \text{atan2}(\mathbf{x}), \quad (47a)$$

$$r_2(\mathbf{x}) := 10^{-1} \sin(10 \cdot \theta(\mathbf{x})) \cdot \mathbf{x}, \quad (47b)$$

where $\text{atan2}(\mathbf{x})$ denotes the $(-\pi, \pi]$ -valued angle between \mathbf{x} and the $[1 \ 0]$ -axis (cf. Figure 3). We choose $\gamma = 0.1$ and $T = 1$ as final simulation time. The resulting ALE formulation is discretized using a first-order finite element approximation with 3,988 degrees of freedom per spatial variable, i.e. 11,964 degrees of freedom in total. As time step size we choose $\Delta t = 0.01$.

The solution trajectories of the solution fields \hat{u}_h^n and Ψ_h^n are visualized in Figure 4 for $\mu^* = (0.1, 0.1, 1, 1)$. The corresponding reconstruction u_h^n on the deformed domain Ω_h^n is shown in Figure 1.

The discrete model and its reduction was implemented using `NGSolve` [29] and `pyMOR` [19]. All computations were performed on a single core of dual-socket Intel Xeon E5-2698 compute server with 256GB RAM.

5.1 Lagrangian vs. Eulerian viewpoint

To assess the viability of our approach, consider for the same parameter μ^* the embeddings

$$A_h^n : L^2(\Omega_h^n) \longrightarrow L^2(\mathbb{R}^2) \quad (48)$$

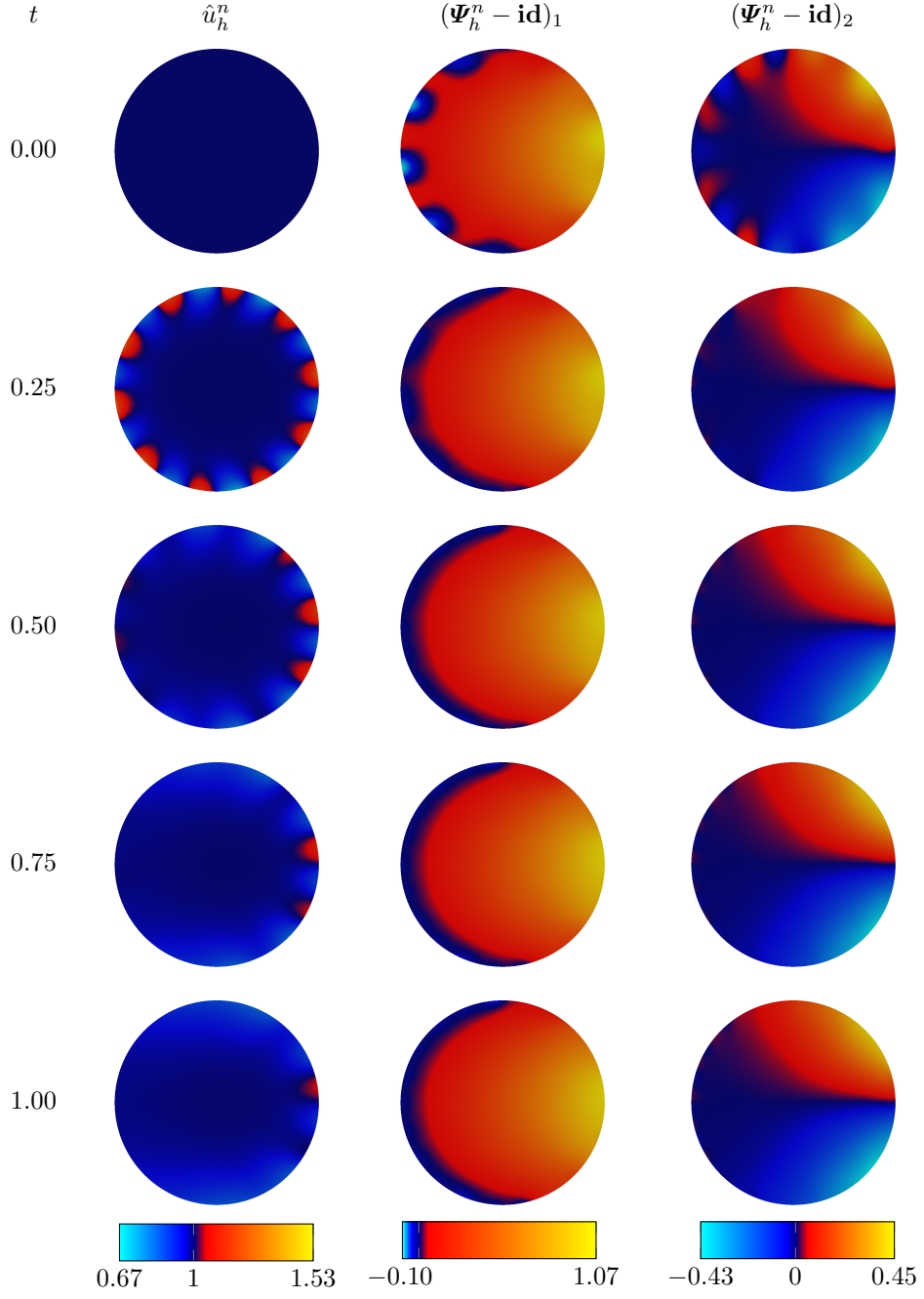
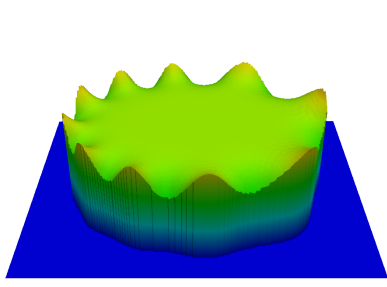
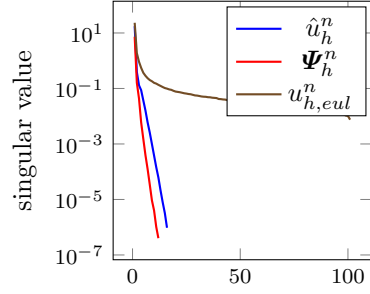


Figure 4: Solution of the ALE discretization of the example problem for parameters $\alpha = 0.1$, $\beta = 0.1$, $\delta_1 = 1$, $\delta_2 = 1$. Depicted are the concentration field \hat{u}_h^n as well as the scalar components of the deformation field $\Psi_h^n - \mathbf{id}$ for different times t .



(a) Eulerian embedding of the concentration field trajectory $u_{h,eul}^n$ at time $t = 0.25$.



(b) Singular value decay of the concentration and transformation field trajectories \hat{u}_h^n , Ψ_h^n vs. Eulerian concentration field trajectory $u_{h,eul}^n$.

Figure 5: Eulerian embedding and singular value decay for the solution trajectory depicted in Figure 4.

given by extending functions on Ω_h^n with zero outside of Ω_h^n . To numerically approximate this mapping we consider a fixed reference mesh on a sufficiently large domain containing $\bigcup_{0 \leq n \leq N} \Omega_h^n$ and compute the first order finite element functions $u_{h,eul}^n$ on this mesh given by Lagrange interpolation of u_h^n (cf. Figure 5a). These functions $u_{h,eul}^n$ can be seen as representatives for solution trajectories of discretizations of (1) that take an Eulerian viewpoint, as opposed to the presented Lagrangian formulation, e.g. phase-field discretizations with the size of the diffuse interface tending to zero.

In Figure 5b we compare the singular value decay of the Lagrangian solution field trajectories \hat{u}_h^n , Ψ_h^n to the singular value decay of the Eulerian concentration field trajectory $u_{h,eul}^n$. As expected, due to the smooth time dependence of \hat{u}_h^n and Ψ_h^n , both trajectories show a much faster singular value decay compared to the $u_{h,eul}^n$ trajectory, which is non-differentiable in time due to its moving jump at the boundary of Ω_h^n .

Remark 1 We notice that exchanging the extensions Λ_h^n in (48), e.g. applying recent ideas from unfitted finite elements [16] to compute smooth extensions of the concentration field outside of $\Omega(t)$, may improve the approximability for the Eulerian formulation. However, even if the approximability can be improved drastically, it is unclear how hyper-reduction can be effectively applied (i.e. with a small number of interpolation points) in such an unfitted setting.

In [2] a different approach is taken, effectively considering the approximation problem over multiple spaces, by truncating approximating vectors defined on $L^2(\mathbb{R}^n)$ to the respective domain $\Omega(t)$.

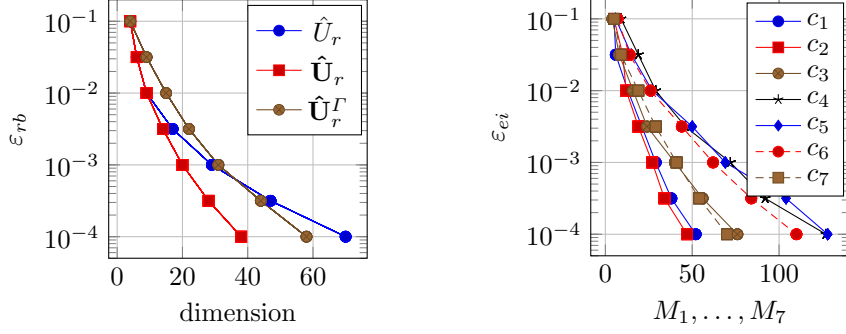


Figure 6: Reduced space dimensions (left) and number of empirical interpolation points (right) vs. training tolerance for the numerical experiment.

5.2 Parametric model order reduction

To test the parameterized model order reduction approach discussed in Section 4, we consider the parameter domain

$$(\alpha, \beta, \delta_1, \delta_2) \in \mathcal{P} := [0.1, 1] \times [0.001, 0.1] \times [0, 1]^2 \subset \mathbb{R}^4, \quad (49)$$

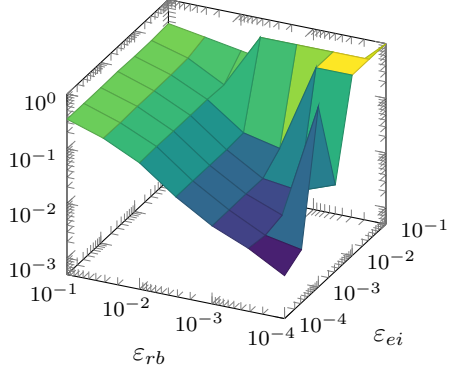
of which we choose a training set $\mathcal{S}_{train} \subset \mathcal{P}$ of 3^4 equidistant parameters. From the corresponding snapshot trajectories we compute the reduced approximation spaces \hat{U}_r , $\hat{\mathbf{U}}_r$, $\hat{\mathbf{U}}_r^F$ and empirical interpolations of c_1, \dots, c_7 for varying relative training error tolerances ε_{rb} , ε_{ei} (cf. Figure 6). To assess the quality of the resulting ROMs, we compute the maximum relative model order reduction errors for 100 randomly chosen test parameters $\mathcal{S}_{test} \subset \mathcal{P}$ (cf. Figure 7). We can observe an exponential error decay in both solution variables for simultaneously decreasing training error tolerances. For $\varepsilon_{rb} = \varepsilon_{ei} = 10^{-3}$ we observe errors of $1.36 \cdot 10^{-2}$ for $\hat{u}_{r,\mu}^n$ and of $2.99 \cdot 10^{-3}$ for $\hat{\Psi}_{r,\mu}^n$. For $\varepsilon_{ei} \gg \varepsilon_{rb}$ we observe the usual instability of ROMs employing empirical interpolation for hyper-reduction. The computational speedup of the ROM over the finite element ALE discretization is shown in Figure 8b (surface plot). For $\varepsilon_{rb} = \varepsilon_{ei} = 10^{-3}$ the speedup is 41.

Next we consider the effect of not enforcing total mass conservation of the ROM: Whereas all previous computations were performed using the mass conservative concentration update equation (45), we now compute solutions of the ROM obtained using (33b) for the concentration update and consider the maximum relative mass conservation error

$$\frac{|\int_{\Omega_{r,\mu}^N} \hat{u}_{r,\mu}^n d\mathbf{x} - \int_{\Omega_{r,\mu}^0} \hat{u}_{r,\mu}^0 d\mathbf{x}|}{\int_{\Omega_{r,\mu}^0} \hat{u}_{r,\mu}^0 d\mathbf{x}} \quad (50)$$

over all $\mu \in \mathcal{S}_{test}$ (Figure 8a). We observe that the error decays with, but is almost always larger than ε_{ei} , whereas it is mostly independent of ε_{rb} . At the same time, computing (33b) instead of (45) is only slightly faster (Figure 8b, mesh plot). For

Model Order Reduction Error – $\hat{u}_{r,\mu}^n$



Model Order Reduction Error – $\Psi_{r,\mu}^n$

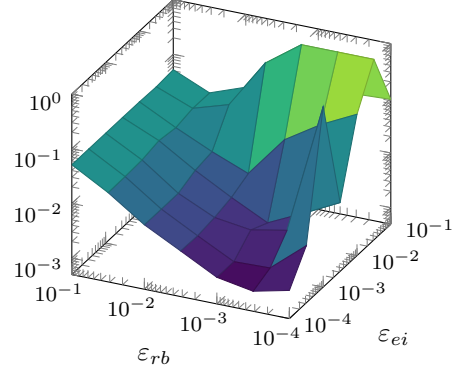


Figure 7: Model order reduction errors for the numerical experiment. Depicted is the maximum relative error over all $0 \leq n \leq N$ and $\mu \in \mathcal{S}_{test}$ for a test set $\mathcal{S}_{test} \subset \mathcal{P}$ of 100 randomly chosen parameters. The errors were truncated at a maximum value of 1 to improve the readability of the plots.

$\varepsilon_{rb} = \varepsilon_{ei} = 10^{-3}$ the speedup grows from 41 to 43. The model order reduction errors are of the same order of magnitude.

One important use case of parametric model order reduction is to quickly compute a certain quantity of interest from the state-space solution of the ROM. As an example, we here consider the variance of the concentration field $\hat{u}_{r,\mu}^n$

$$V_{r,\mu}^n := \frac{\int_{\Omega_{r,\mu}^n} (\hat{u}_{r,\mu}^n - \bar{u}_{r,\mu}^n)^2 d\mathbf{x}}{\int_{\Omega_{r,\mu}^n} 1 d\mathbf{x}}, \quad \bar{u}_{r,\mu}^n := \frac{\int_{\Omega_{r,\mu}^n} u_{r,\mu}^n d\mathbf{x}}{\int_{\Omega_{r,\mu}^n} 1 d\mathbf{x}}, \quad (51)$$

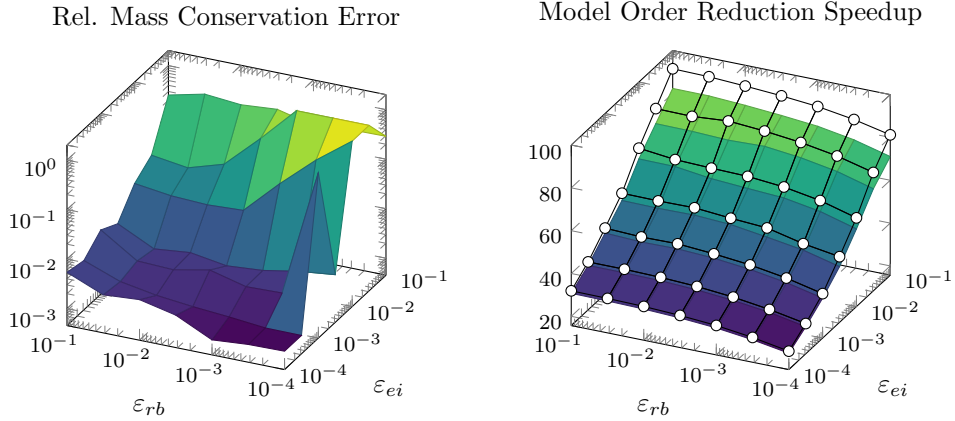
which can be computed from the ROM as

$$V_{r,\mu}^n = \frac{\tilde{a}_3(\hat{u}_{r,\mu}^n - \bar{u}_{r,\mu}^n, \hat{u}_{r,\mu}^n - \bar{u}_{r,\mu}^n; \Psi_{r,\mu}^n)}{\tilde{a}_3(1, 1; \Psi_{r,\mu}^n)}, \quad \bar{u}_{r,\mu}^n = \frac{\tilde{a}_3(\hat{u}_{r,\mu}^n, 1; \Psi_{r,\mu}^n)}{\tilde{a}_3(1, 1; \Psi_{r,\mu}^n)}. \quad (52)$$

In Figure 9 we have computed $V_{r,\mu}$ for $\varepsilon_{rb} = \varepsilon_{ei} = 10^{-3}$ and 50×50 equidistant values of δ_1 and δ_2 whereas $\alpha = \beta = 0.1$ were fixed. The computation of these 2,500 outputs took 36 minutes.

Conclusion and outlook

We presented the application of projection-based model order reduction for a model free boundary problem with unknown evolving geometry. By using ALE mappings to describe the geometry evolution of the model, we were able to apply standard reduced basis and empirical interpolation techniques. An appropriate time discretization



(a) Maximum relative errors in mass conservation (50) for $\mu \in \mathcal{S}_{test}$ when using (33b) for the concentration update. The errors were truncated at a maximum value of 1 to improve the readability of the plots.

(b) Median of model order reduction speedup over $\mu \in \mathcal{S}_{test}$. Surface plot: concentration update using (45); mesh plot: concentration update using (33b).

Figure 8: Total mass conservation errors and model order reduction speedups for the numerical experiment (cf. Figure 7).

allowed us to obtain a globally mass conservative Galerkin ROM by including the constant functions in the reduced state space. Through a rank-one modification of the empirically interpolated reduced mass matrix we could preserve this property in the final fully online-efficient Galerkin-EI ROM.

In this work we have focussed on the reduced order modeling aspects specific to free boundary problems. The integration of more advanced techniques such as greedy basis generation based on a posteriori error indicators for the ROM should be straightforward.

We believe that the methodology can also be applied to different and even more complex free boundary problems. However, an obvious limitation of the presented approach lies in the dependency on one reference domain w.r.t. which all other domains can be expressed. For problems with large deformations or topology changes this will be insufficient and different discretizations with suitable reduced order modeling have to be considered.

Without changing the general approach, remeshing in the high-dimensional problem could be considered by considering multiple meshes on the reference domain $\hat{\Omega}$ and using reduced basis techniques for mesh-adaptive schemes such as [35, 33, 1, 11]. However in the presence of large deformations, $\Omega(t)$ -dependent norms will have to be considered in the schemes in contrast to the currently fixed function spaces norms w.r.t. the reference domain.

Very attractive for the discretization would be the use of unfitted (or embedded)

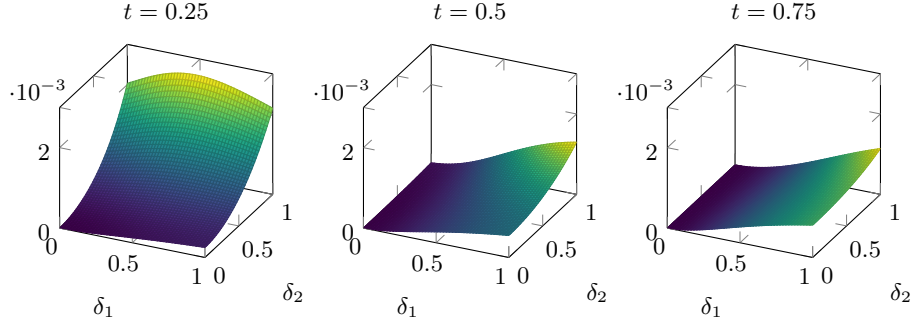


Figure 9: Variance $V_{r,\mu}^n$ (51) of the concentration field $\hat{u}_{r,\mu}^n$ for 50×50 combinations of the deformation parameters δ_1, δ_2 , $\alpha = 0.1$, $\beta = 0.1$.

discretizations. In such a setting a naive approximation fails as we have seen in Section 5.1. It would be interesting if the slow decay of the Kolmogorov n -widths could be repaired by choosing a suitable embedding to define a joint approximation space (see also Remark 1). How hyper-reduction could be effectively applied in such an approach is unclear, however.

Software availability

The source code used to produce the numerical results in Section 5 can be obtained from <https://doi.org/10.5281/zenodo.1232550> under an open source license.

References

- [1] Mazen Ali, Kristina Steih, and Karsten Urban. Reduced basis methods based upon adaptive snapshot computations. *Advances in Computational Mathematics*, 43(2):257–294, 2017.
- [2] Maciej Balajewicz and Charbel Farhat. Reduction of nonlinear embedded boundary models for problems with evolving interfaces. *Journal of Computational Physics*, 274:489–504, 2014.
- [3] Francesco Ballarin and Gianluigi Rozza. POD-Galerkin monolithic reduced order models for parametrized fluid-structure interaction problems. *International Journal Numerical Methods for Fluids*, 82(12):1010–1034, 2016.
- [4] Eberhard Bänsch. Finite element discretization of the Navier–Stokes equations with a free capillary surface. *Numerische Mathematik*, 88(2):203–235, April 2001.
- [5] Maxime Barrault, Yvon Maday, Ngoc Cuong Nguyen, and Anthony T. Patera. An ”empirical interpolation” method: application to efficient reduced-basis

- discretization of partial differential equations. *Comptes Rendus Mathematique*, 339(9):667–672, 2004.
- [6] Peter Benner, Mario Ohlberger, Albert Cohen, and Karen Willcox, editors. *Model Reduction and Approximation*, volume 15 of *Computational Science & Engineering*. SIAM, Philadelphia, PA, 2017.
 - [7] Kevin Carlberg, Youngsoo Choi, and Syuzanna Sargsyan. Conservative model reduction for finite-volume models. *arXiv:1711.11550*, 2017.
 - [8] Jean Donea, Antonio Huerta, Jean-Philippe Ponthot, and Antonio Rodriguez-Ferran. Chapter 14: Arbitrary Lagrangian-Eulerian Methods. In Erwin Stein, René Borst, and Thomas J.R. Hughes, editors, *Encyclopedia of Computational Mechanics Vol. 1: Fundamentals*. Wiley & Sons, 2004.
 - [9] Avner Friedman. Free boundary problems in biology. *Philosophical Transactions of the Royal Society A*, 373(2050):20140368, 2015.
 - [10] Kurt Frischmuth and Michael Hänler. Numerical analysis of the closed osmometer problem. *ZAMM-Journal of Applied Mathematics and Mechanics*, 79(2):107–116, 1999.
 - [11] Carmen Gräßle and Michael Hinze. The combination of POD model reduction with adaptive finite element methods in the context of phase field models. *PAMM*, 17(1):47–50, 2017.
 - [12] Jan S Hesthaven, Gianluigi Rozza, and Benjamin Stamm. *Certified Reduced Basis Methods for Parametrized Partial Differential Equations*. SpringerBriefs in Mathematics. Springer International Publishing, 2016.
 - [13] Michael Hinze, Joachim Krenciszek, and René Pinnau. Proper orthogonal decomposition for free boundary value problems. *Hamburger Beiträge zur Angewandten Mathematik*, 2014-17, 2014.
 - [14] Cyrill W. Hirt, Anthony A. Amsden, and J. L. Cook. An arbitrary Lagrangian–Eulerian computing method for all flow speeds. *Journal of Computational Physics*, 14(3):227–253, 1974.
 - [15] Toni Lassila, Alfio Quarteroni, and Gianluigi Rozza. A reduced basis model with parametric coupling for fluid-structure interaction problems. *SIAM Journal on Scientific Computing*, 34(2):A1187–A1213, 2012.
 - [16] Christoph Lehrenfeld and Maxim A. Olshanskii. An Eulerian finite element method for PDEs in time-dependent domains. *arXiv:1803.01779*, 2018.
 - [17] Friedrich Lippoth and Georg Prokert. Classical solutions for a one-phase osmosis model. *Journal of Evolution Equations*, 12(2):413–434, 2012.
 - [18] Friedrich Lippoth and Georg Prokert. Stability of equilibria for a two-phase osmosis model. *NoDEA Nonlinear Differ. Equ. Appl*, 21:129–149, 2014.

- [19] René Milk, Stephan Rave, and Felix Schindler. pyMOR – Generic Algorithms and Interfaces for Model Order Reduction. *SIAM Journal on Scientific Computing*, 38(5):S194–S216, 2016.
- [20] M. Ohlberger and F. Schindler. Error control for the localized reduced basis multiscale method with adaptive on-line enrichment. *SIAM J. Sci. Comput.*, 37(6):A2865–A2895, 2015.
- [21] Mario Ohlberger and Stephan Rave. Nonlinear reduced basis approximation of parameterized evolution equations via the method of freezing. *Comptes Rendus Mathématique*, 351(23–24):901–906, 2013.
- [22] Mario Ohlberger and Stephan Rave. Reduced basis methods: Success, limitations and future challenges. In *Proceedings of ALGORITMY 2016, 20th Conference on Scientific Computing, Vysoke Tatry, Podbanske, Slovakia, March 13-18, 2016*, pages 1–12. Publishing House of Slovak University of Technology in Bratislava, 2016.
- [23] Stanley Osher and Ronald Fedkiw. *Level set methods and dynamic implicit surfaces*, volume 153. Springer Science & Business Media, 2006.
- [24] Goran Peskir and Albert Shiryaev. *Optimal stopping and free-boundary problems*. Springer, 2006.
- [25] Christophe Prud’homme, Dimitrios V. Rovas, Karen Veroy, Lieven Machiels, Yvon Madaay, Anothony T. Patera, and Gabriel Turinici. Reliable real-time solution of parametrized partial differential equations: Reduced-basis output bound methods. *Journal of Fluids Engineering*, 124(1):70–80, 2001.
- [26] Alfio Quarteroni, Andrea Manzoni, and Federico Negri. *Reduced Basis Methods for Partial Differential Equations*, volume 92 of *La Matematica per il 3+2*. Springer International Publishing, 2016.
- [27] Andreas Rätz. Diffuse-interface approximations of osmosis free boundary problems. *SIAM Journal on Applied Mathematics*, 76(3):910–929, 2016.
- [28] Magnus Redeker and Bernard Haasdonk. A POD-EIM reduced two-scale model for crystal growth. *Advances in Computational Mathematics*, 41(5):987–1013, 2015.
- [29] J. Schöberl. C++11 Implementation of Finite Elements in NGSolve. *Institute for Analysis and Scientific Computing, Vienna University of Technology*, 2014.
- [30] James Albert Sethian. *Level set methods and fast marching methods: evolving interfaces in computational geometry, fluid mechanics, computer vision, and materials science*, volume 3. Cambridge University Press, 1999.
- [31] Lawrence Sirovich. Turbulence and the dynamics of coherent structures part I: Coherent structures. *Quarterly of Applied Mathematics*, 45(3):561–571, 1987.

- [32] Johan Stefan. Über die Theorie der Eisbildung, insbesondere über die Eisbildung im Polarmeere. *Annalen der Physik*, 278(2):269–286, 1891.
- [33] Sebastian Ullmann, Marko Rotkvic, and Jens Lang. POD-Galerkin reduced-order modeling with adaptive finite element snapshots. *Journal of Computational Physics*, 325:244–258, 2016.
- [34] S. Volkwein. Optimal control of a phase-field model using proper orthogonal decomposition. *ZAMM – Journal of Applied Mathematics and Mechanics / Zeitschrift für Angewandte Mathematik und Mechanik*, 81(2):83–97, 2001.
- [35] M. Yano. A minimum-residual mixed reduced basis method: Exact residual certification and simultaneous finite-element reduced-basis refinement. *ESAIM Math. Model. Numer. Anal.*, 50(1):163–185, 2016.
- [36] Martijn Maria Zaal. Cell swelling by osmosis: A variational approach. *Interfaces and Free Boundaries*, 14(4):487–521, 2012.
- [37] Martijn Maria Zaal. *Variational modeling of parabolic free boundary problems*. PhD thesis, University of Amsterdam, 2013.
- [38] Martijn Maria Zaal. Well-posedness of a parabolic free boundary problem driven by diffusion and surface tension. *Mathematical Methods in the Applied Sciences*, 38(2):380–392, 2015.